Understanding the Effects of Subsidence on Unconfined Aquifer Parameters by Integration of Lattice Boltzmann Method (LBM) and Genetic Algorithm (GA)

Roghayeh Yousefi (r.yousefi@shirazu.ac.ir)
Shiraz University https://orcid.org/0000-0002-3219-8723
Nasser Talebbeydokhti
Shiraz University
Seyyed Hosein Afzali
Shiraz University
Maryam Dehghani
Shiraz University
Ali Akbar Hekmetzadeh
Shiraz University of Technology

Research Article

Keywords: Unconfined Aquifer Parameters, Subsidence, Lattice Boltzmann Method, Genetic Algorithm, Inverse Solution, Groundwater Flow

Posted Date: March 14th, 2022

DOI: https://doi.org/10.21203/rs.3.rs-1428553/v1

Understanding the Effects of Subsidence on Unconfined Aquifer parameters by Integration of Lattice Boltzmann Method (LBM) and Genetic Algorithm (GA)

Roghayeh Yousefi, Nasser Talebbeydokhti, Seyyed Hosein Afzali, Maryam Dehghani, Ali Akbar Hekmetzadeh

Abstract

Excessive exploitation of groundwater has led to a significant subsidence in Darab plain, located in Fars province, Iran. The compaction of aquifer layers especially in fine-grain sediments leads to changes in aquifer parameters including hydraulic conductivity, specific yield, and compressibility which consequently changes the permeability and storage of the aquifer. Accordingly, a precise estimation of aquifer parameters are essential for both future water resources planning and management. The main objective of this paper is to determine the most optimum values of aquifer parameters based on the groundwater information and subsidence measurements spanning from 2010 to 2016. The proposed approach for inverse solution of groundwater flow is based on Lattice Boltzmann Method (LBM) integrated with Genetic Algorithm for optimization (GA). Subsidence measurements made by previous studies as well as the initial values of unknown parameters obtained from piezometric information are incorporated into the inverse modeling. The whole process of inverse modeling is repeated from 2010 to 2016 which leads to annually estimation of the aquifer parameters. Due to the compaction occurring in the aquifer system, a decreasing temporal trend is observed in the aquifer parameters in most parts of the plain. By fitting a function to time-dependent aquifer parameters, their corresponding values and consequently the amount of subsidence in 2017 are predicted. The small average relative error (~3.5%) between the predicted land subsidence and the measurements demonstrates the high performance of the proposed inverse modeling approach.

Keywords: Unconfined Aquifer Parameters, Subsidence, Lattice Boltzmann Method, Genetic Algorithm, Inverse Solution, Groundwater Flow

Research highlights

- LBM and GA were integrated to find the parameters of Darab unconfined aquifer
- Compressibility equation as a link between subsidence and groundwater was used
- The hydraulic conductivity and specific yield are decreased over the time
- The predicted parameters were used to estimate the land subsidence in future

1. Introduction

In recent decades, various numerical methods have been developed as essential tools to study the groundwater flow. Nearly all groundwater flow equations consist of partial differential equations as a function of aquifer parameters such as hydraulic conductivity and storage coefficient. An accurate knowledge of the aquifer parameters are of essential importance for groundwater flow prediction. Determining the aquifer parameters based on hydraulic head as observations is known as 'inverse solution of the groundwater flow' (Garcia and Shigidi 2007). Various researches have been conducted to address the problem of aquifer parameters estimation and calibration. In recent years, the inversion methods based on optimization have received special attention due to their efficiency and simplicity. The optimization approaches such as Genetic Algorithm (GA) basically employ a search method to find the unknown parameters that minimize the difference between observed and calculated head values (Hana et al. 2020). GA is widely used in the optimization problems due to their specific advantages such as easy convergence to the global optimal solution and high accuracy (Ayaz 2017). Mahinthakumar and Sayeed used the real encoded genetic algorithm (RGA) and the binary encoded genetic algorithm (BGA) to integrate with different search methods to understand the location and release intensity of the two-dimensional pollution area (2005).

Significant endeavors have been made to solve the inverse problems and automate the calibration process for aquifer parameters estimation (Sonnenborg et al. 2003; Geza et al. 2009; Abdelaziz & Merkel 2015; Lu et al. 2014). For instance, GA was employed to solve the inverse problem by Gentry et al. (2003) in a semi-confined aquifer. In another study, GA is jointly applied with a groundwater modeling as an innovative model of groundwater pollution sources to identify the parameters of groundwater pollution sources. (Aral et al. 2001). The GA optimization was combined with transport model by Ayaz (2017) and integrated with MODFLOW and MT3DMS models by Sophia and Bhattacharjya (2020) to simulate the groundwater contaminant transport.

In addition to the above considerations, the solution of the groundwater flow equation is another issue to be addressed for parameters estimation. The lattice Boltzmann method (LBM) as an innovative numerical method in hydraulic problems (Ru et al. 2021), is one approach in this regard. The LBM is identified with its comfort of performance, parallel processing ability, and easy handling of boundary conditions which make it an appropriate method to simulate the complicated flows with complex boundaries (Budinski et al. 2015). The first application of the LBM was implemented by Gladrow (Gladrow 1994) who proposed Lattice Boltzmann equation (LBE) models for diffusion instead of lattice gas automata due to its greater flexibility and freedom. The LBM has been successful performance in fluid flow modelling such as Navier–Stokes (Ansumali et al. 2007), shallow water [Liu

et al. 2013, Peng et al. 2011, Zhou 2004], groundwater (Zhou 2007a; Zhou 2011; Budinski et al. 2015; Arsyad et al. 2017; Hekmatzadeh et al. 2018; 2019), and especially multiphase flow in porous media [Anwar and Sukop 2008; Fattahi et al. 2016; Gharibi and Ashrafizaadeh 2020). LBM has been widely applied to explore heat and mass transfer problems such as pollutant transport (Lei et al. 2013), thermal response (Gao et al. 2021), saltwater intrusion (Servan-Camas and T.-C. Tsai 2009) and reaction diffusion (Lin et al. 2021).

Recently, much attention has been paid to use the LBM for modeling the fluid flows and various researches have been conducted to solve advection, diffusion, dispersion and groundwater equations (Zhou 2011). Modeling the fluid flow through porous media is of great importance especially because of its applications in oil extraction, groundwater contamination, storage of nuclear waste, and chemical reactors (Fattahi et al. 2016). In one study, Zhou investigated the applicability of the LBM to isotropic groundwater flow modeling in confined aquifers (Zhou 2007a, b; Budinski et al. 2015). Moreover, it has been shown that the LBM is an efficient numerical approach used to solve the groundwater flow in unconfined aquifer as well (Yousefi et al. 2020).

By incorporating GA optimization into an approach for groundwater flow solution such as LBM, we will be able to take the advantages of both methods to estimate the aquifer parameters. This is the main novelty of this paper which is characterization of the aquifer system by integration of LBM and GA optimization in Darab plain, Iran. Severe groundwater exploitation has led to a significant land subsidence in Darab plain as a result of fine-grained sediments compaction occurred in the aquifer (Yousefi et al. 2019). Land subsidence definitely affects the hydrology and hydrogeology properties of aquifer system. Hence, incorporation of the subsidence amount into the inverse solution of the groundwater flow is of significant importance. The aquifer parameters including hydraulic conductivity, specific yield and compressibility are yearly estimated using the proposed method of inverse solution and the annual measurements of the subsidence. The temporal trends of the aquifer parameters are further investigated to predict the parameters values associated with a desired time. This process is followed by prediction of the corresponding subsidence which is finally compared to the observed value.

1.2. Case study

Darab plain is located in Fars province (Iran) with the area of 2400 km^2 (Fig.1) surrounded by high mountains (Regional Water Company of Fars, 2016). The average temperature ranges from 14˚ C to 22˚ C and the average annual rainfall is recorded as 245 mm. The aquifer system in this plain is unconfined and the number of pumping wells located in the area is 3444 (Regional Water Company of Fars 2016). Over a period of 23 years (1993–2016), the groundwater level in the plain has dropped 26 m. The most amount of groundwater exploitation is due to

farmlands irrigation. Due to the decrease of groundwater level, Darab plain is subject to land subsidence which is mostly happening in the agricultural lands in the main part of the plain (Fig. 1).

Fig.1. Location of the aquifer system in the Darab plain superimposed on the LANDSAT 8 OLI color composite image (R:7, G:4, B:2). The yellow stars represent the piezometric wells while the green areas in the black polygon indicate the agricultural lands

Land subsidence happens due to the fine-grained sediments compaction as a result of increasing effective stress. The compaction occurred in the fine-grained interbeds, will influence the aquifer parameters including specific yield, compressibility and hydraulic conductivity. A precise knowledge of the aquifer parameters and their relationship with the compaction mechanism will enable us to predict the subsidence occurrence.

The primary objective of this paper is to present a novel method based on a combination of LBM and GA to solve the inverse groundwater flow equation for 2D problem in order to precisely estimate the aquifer parameters. To do so, initial values of the parameters and other required quantities are first extracted from the existing reports on groundwater information. Fig. 2 indicates the initial amounts of hydraulic conductivity which ranges from 0.32 (m/day) and 18.31 (m/day) in the center and north of the area, respectively (Regional Water Company of Fars 2016).

Fig.2. Initial hydraulic conductivity (m/day) of Darab aquifer system

Hydraulic head extracted from the piezometric information of 2010 is also shown in Fig. 3. According to this figure, the north and south parts of the area are inflow and outflow boundaries, respectively, while there is no flow border in east and west direction (solid boundary).

Fig.3. Hydraulic head in Darab aquifer system

Moreover, the thickness of the Darab aquifer system obtained from the piezometric information is illustrated in Fig. 4. The maximum thickness of 250m belongs to the center of the plain which decreases to 20 m towards the area boundaries (Regional Water Company of Fars 2016).

Fig.4. Thickness (m) of Darab aquifer system

In previous studies, the temporal behavior and spatial extent of the subsidence has been investigated by Yousefi et al. (2019) using Synthetic Aperture Radar Interferometry (InSAR). Two different SAR satellite images, Envisat ASAR and Sentinel-1A (spanning 2010 and 2015 – 2017) have been employed to extract the subsidence rate. As suggested by both datasets, there are three main subsidence lobes with different deformation rate as depicted in Fig. 5 (Yousefi, et al. 2019).

Fig.5. Subsidence velocity maps obtained from: (a) ENVISAT ASAR and (b) Sentinel-1A (Yousefi et al. 2019)

It is supposed to apply the subsidence maps to infer the aquifer parameters by inverse modeling of groundwater flow expressed in the LBM framework. The rationale behind the LBM and its usage for modeling the groundwater flow is first explained in below followed by the inverse modeling workflow.

2. Lattice Boltzmann Method (LBM) for Modeling the Groundwater Flow

General form of the 2D groundwater flow equation in unconfined aquifer is defined as (Budinski et al. 2015):

$$\frac{\partial h}{\partial t} = \frac{K}{S_y}\left(\frac{\partial^2 (h^2/2)}{\partial x_i^2}\right) + \frac{R}{S_y} \quad (1)$$

where K and S_y indicate the hydraulic conductivity and specific yield, h and R are the groundwater head and the recharge function, respectively and x_i, shows two directions in the horizontal plane. The groundwater flow equation in unconfined aquifer which is solved in the form of LBM (Eq. 2) is represented as (Yousefi et al. 2021):

$$f_k(x+c_k\,\Delta t, t+\Delta t) = f_k(x,t) + \frac{1}{\tau}[f_k^{eq}(x,t) - f_k(x,t)] + \frac{R}{a\,S_y}\Delta t \tag{2}$$

where f_k and f_k^{eq} represent the particle distribution function and the local equilibrium distribution function, respectively, Δt is the time step, x is a vector in xy coordinate system, c_k is the particle velocity vector, τ is the single relaxation time, and a is the number of the particle. In this study, D2Q9 lattice configuration is applied to model the groundwater flow using LBM (Fig.6), and accordingly, $a = 9$. Moreover, c_k, indicates the velocity and is described as follows; ($c_x = \Delta x/\Delta t$) (Zhou 2004):

$$c_k = \begin{cases} (0,0) & k = 0 \\ (\pm c_x, 0), (0, \pm c_y) & k = 1, 2, 3, 4 \\ (\pm c_x, \pm c_y) & k = 5, 6, 7, 8 \end{cases} \tag{3}$$

Fig.6. Nine-velocity rectangular lattice (D2Q9) (Mohammad 2011)

f_k is also specified as:

$$f_k(x,t) = w_k h(x,t) \tag{4}$$

where, $h(x,t)$ and w are groundwater hydraulic head and weight factor, respectively for each direction according to the next terms. The weight factors are indicated as:

$$\begin{aligned} &w_0 = \frac{4}{9} \quad , \\ &w_1 = w_2 = w_3 = w_4 = \frac{1}{9} \quad , \\ &w_5 = w_6 = w_7 = w_8 = \frac{1}{36} \end{aligned} \tag{5}$$

Four types of boundary conditions are applied in the simulation of groundwater flow, including the Dirichlet, Neumann, open and solid boundary conditions in line with Eq. (6) to Eq. (9).

Fig.7. Solid boundary condition (Mohammad 2011)

According to Fig.7, the distribution functions at solid boundary (south boundary) are computed by Eq.(6) as follows:

$$f_2 = f_4 \ , \ f_5 = f_7 \ , \ f_6 = f_8 \tag{6}$$

Assuming open boundary for the east boundary in Fig.7, Eq. (7) is employed for calculating the distribution functions:

$$\begin{aligned} f_3(i=m,j) &= 2\times f_3(i=m-1,j) - f_3(i=m-2,j) \\ f_6(i=m,j) &= 2\times f_6(i=m-1,j) - f_6(i=m-2,j) \\ f_7(i=m,j) &= 2\times f_7(i=m-1,j) - f_7(i=m-2,j) \end{aligned} \tag{7}$$

Dirichlet boundary condition at the west boundary in Fig.7 suggests Eq. (8) to measure the distribution functions:

$$\begin{aligned} f_1 &= (w_1 + w_3)\times h - f_3 \\ f_5 &= (w_5 + w_7)\times h - f_7 \\ f_8 &= (w_8 + w_6)\times h - f_6 \end{aligned} \tag{8}$$

Regarding the case of Neumann Boundary condition (north boundary in Fig.7) the distribution function is estimated by Eq. (9) as follows:

$$\begin{aligned} f_4(i.j=n) &= f_4(i.j=n-1) \\ f_7(i.j=n) &= f_7(i.j=n-1) \\ f_8(i.j=n) &= f_8(i.j=n-1) \end{aligned} \tag{9}$$

Apart from the boundary conditions, the following equations have been already introduced as the equilibrium distribution function for unconfined aquifers (Yousefi et al. 2021):

$$\begin{aligned} f_k^{eq} &= h - \frac{K}{S_y}\left(\frac{1}{\Delta t\, c^2(\tau-0.5)}\right)\frac{h^2}{2} && k=0 \\ f_k^{eq} &= \frac{1}{4}\frac{K}{S_y}\left(\frac{1}{\Delta t\, c^2(\tau-0.5)}\right)\frac{h^2}{2} && k=1,2,3,4 \\ f_k^{eq} &= -\frac{K}{S_y}\left(\frac{1}{4\Delta t\, c_{kx}c_{ky}(\tau-0.5)}\right)\frac{h^2}{2} && k=5,6,7,8 \end{aligned} \tag{10}$$

Eqs. (10) are characterized by the following relations:

$$\sum_k f_k^{eq}(x,t) = h(x,t) \tag{11}$$

$$\sum_k c_{ki} f_k^{eq}(x,t) = 0 \tag{12}$$

$$\sum_k c_{ki} c_{kj} f_k^{eq}(x,t) = \frac{(\frac{K}{S_y})_{ij}}{\Delta t(\tau - 0.5)} \frac{h^2(x,t)}{2} \tag{13}$$

By taking into account Eqs. (3) to (13), the groundwater flow can be modeled using Eq. (2) which is a function of aquifer parameters, i.e. K and S_y as well as the aquifer compressibility (α). The initial values of K, S_y and α are first estimated using the piezometric measurements followed by calibrating the relaxation time. The optimized aquifer parameters are then estimated using (GA) by freezing the amount of relation time in the LBM equation. The whole process will be explained in more details in the following section.

3. Proposed Methodology to Estimate the Aquifer Parameters

The whole workflow applied to inverse modeling of groundwater flow for determination of the aquifer parameters of the study area is represented in Fig. 8.

Fig.8. Block diagram of the proposed methodology for aquifer parameters estimation

The first parameter to be calibrated is the relaxation time with a little range of variation. An approximate amount of aquifer parameters, K, S_y and α, would suffice to estimate the relaxation time. The first attempt, hence, is to estimate the compressibility, α, using the relationship between the groundwater level and the land subsidence (aquifer compaction) at piezometric wells location. Knowing about the compressibility would help approximate S_y and the sediment types. In addition, a rough estimate of K is already available from the existing reports. These values are further employed to solve the inverse groundwater flow equation using LBM which is combined with GA in order to estimate the precise values of aquifer parameters.

3.1. Estimation of Approximate Values of Aquifer Parameters using the Relationship between Land Subsidence and Piezometric Information

In order to determine the approximate values of aquifer parameters, the relationship between land subsidence and groundwater level drop in an unconfined aquifer is defined using one dimensional compressibility equation (Eq. 14) (Hoffmann et al. 2003):

$$\alpha = \frac{-db/b}{d\sigma'_{zz}} \tag{14}$$

Where α is compressibility, db is the amount of subsidence, b is the thickness of aquifer and $d\sigma'$ is the effective stress increase. By replacing the amount of effective stress in Eq. 14, the new equation for compressibility is obtained as follows:

$$\alpha = \frac{db/b}{\rho g\, dh} \tag{15}$$

Where ρ is the water density, g is the gravity acceleration and dh is the hydraulic head difference which can be replaced by the difference between two piezometric measurements in a specific time period:

$$h_2 - h_1 = \frac{db/b}{\rho g\, \alpha} \tag{16}$$

According to Eq. 16, the hydraulic head is a function of compressibility where the compressibility is also affected by land subsidence. To approximately achieve the compressibility behavior of Darab aquifer system, Eq. 16 is applied by incorporating the amount of subsidence and the variation of hydraulic head at piezometric wells with annual time step. The land subsidence is obtained from the results of InSAR (Yousefi et al. 2019). These results include the land subsidence time series from 2010 to 2017 which specifies the annual amount of subsidence. Based on the approximate values of compressibility, rough estimates of sediment types ($S.T$) and S_y are also obtained (Table 1). S_y is a dimensionless quantity, ranging between 0 and 0.4. Moreover, the maximum amount of compressibility occurs in the main subsidence zone (wells 3, 5, 9, 11), and consequently, the sediment type is mainly fine-grained as clay. On the other hand, despite the significant hydraulic head decrease at some piezometric wells (wells 1, 7, 10, 12), no remarkable subsidence occurs due to existence of coarse-grained sediment type such as gravel.

Table.1 Information of Darab aquifer at piezometric wells (average value from 2010 to 2015)

3.2. Inverse Solution of Groundwater Flow Equation based on LBM Combined with GA

Eq. 16 is utilized for inverse modeling of the groundwater flow using LBM. Regarding this equation, h_2 is assumed to be computed using LBM while h_1 is the initial head. By substitution of h_2 as a final solution of groundwater flow equation based on LBM, Eq. 16 can be written as:

$$h_2 = \sum_k f_k = \frac{db/b}{\rho g \alpha} + h_1 \tag{17}$$

In other words, the final solution of groundwater flow equation based on LBM should satisfy the above relationship. In order to obtain the inverse solution of the groundwater flow equation, a gridded layer with a cell size of 500 m (including 102×50 lattices) and thickness of the aquifer (Fig. 4), is generated. The relaxation time and the time step required for modeling are to be considered as 1.35 and 0.002 day, respectively. The relaxation time is estimated using approximate values of the aquifer parameters. Based on the hydraulic head contour lines of Fig. 3, the north part of the aquifer is inflow boundary with known hydraulic head (Dirichlet boundary). The south boundary is, however, the outflow one whose hydraulic head is not known (Open boundary) whereas, the east and west borders are no flow boundaries (solid boundary). The annual amount of hydraulic head extracted from the piezometric information in addition to the recharge and discharge of the aquifer for the time period of 2010 – 2016 which is determined from the existing reports are used in the process (Regional Water Company of Fars, 2016). The piezometric head corresponding to 2010 is considered as the initial head, h_1. Moreover, the highest and lowest values of rainfall are 400 and 100 mm, at high altitudes and in the plains, respectively. The annual evaporation and annual infiltration of rainfall in the study area are considered to be about 67% and 30% which are equivalent to 120 and 11 MCM, respectively. According to the existing reports, there were 3444 active pumping wells in the study area in 2010, which corresponds to the annual groundwater discharge volume of about 431.36 MCM which is mostly utilized for agricultural irrigation.

Inverse modeling of groundwater flow with three unknown aquifer parameters including K, S_y and α is performed with incorporation of GA optimization. The objective function to be minimized in GA is the relative difference between the calculated hydraulic head from LBM and the one computed using the subsidence value (the right hand of Eq. 17). The initial population size of 50, the number of generation of 300 and the number of elites equal to 5% of the initial population are considered for GA optimization. The lower and upper bounds of the aquifer parameters which are extracted from Table 1 and Fig. 2, are illustrated in Table 2.

Table 2. Lower and upper bounds of the aquifer parameters used for GA optimization

4. Results

By integration of LBM and GA and application of the annual amount of subsidence, K, S_y and α are annually optimized for 2010 to 2016 (Figs. 9-14).

Fig.9. Optimized K, S_y and α in 2010-2011

Fig.10. Optimized K, S_y and α in 2011-2012

Fig.11. Optimized K, S_y and α in 2012-2013

Fig.12. Optimized K, S_y and α in 2013-2014

Fig.13. Optimized K, S_y and α in 2014-2015

Fig.14. Optimized K, S_y and α in 2015-2016

As observed in Figs 9 to 14, the maximum and minimum amounts of K and S_y occur in the north and center of Darab plain, respectively. On the other hand, the maximum value of α is detected in the main zone of the subsidence which are consistent with the geological setting of the area. The annual relative errors between the calculated hydraulic head and the one observed at the locations of piezometric wells are indicated in Table 3.

Table 3. Model misfit as the relative error calculated at the locations of piezometric wells

The maximum and minimum amounts of relative error are 0.0008 and 0.00001 which occur in wells 2, 5, 9, and 11, respectively. The small range of the relative error confirms that the results of the proposed model are strictly consistent with the observed measurements which is an indication of the accurate estimation of the aquifer parameters.

In order to further evaluate the estimated parameters, the corresponding values in 2017 are predicted by investigation of their temporal trend. Figs. 15-17 depict the temporal behavior of K, S_y and α at piezometric wells which can be simply modeled as a function of time.

Fig.15. Model fitted to the values of hydraulic conductivity (k_x) at the locations of piezometric wells in 2010-2016. Solid line illustrates the temporal model.

Fig.16. Model fitted to the values of specific yield (S_y) at the locations of piezometric wells in 2010-2016. Solid line illustrates the temporal model.

Fig.17. Model fitted to the values of compressibility (α) at the locations of piezometric wells in 2010-2016. Solid line illustrates the temporal model.

Figs. 15-17, indicate that the temporal trends of K, S_y, and α, between 2010 and 2016 are mostly decreasing. The values of K and S_y are, however, constant out of the subsidence zones (wells 4, 6, 10, and 12). The compressibility (α) at wells 2, 5, and 12 increases with time while K and S_y are constant or have a decreasing trend. Using the fitted functions at every grid cell, the aquifer parameters corresponding to 2017 are predicted. This process is followed by modeling the subsidence in 2017 using LBM (Fig.18) which can be further evaluated by InSAR measurements.

Fig.18. Predicted subsidence using the anticipated values of the aquifer parameters in 2017

Fig. 19 shows the relative error as the model misfit calculated between the predicted subsidence and the one obtained from InSAR measurements (Yousefi et al. 2019).

Fig. 19. Relative error between the predicted subsidence and InSAR measurements

The maximum relative error is estimated as 15%, which belongs to only 1% of all pixels at boundaries. In the subsidence area, however, the amount of the model misfit is considerably smaller. The averaged relative error of the whole study area is estimated as 3.5% which is an indication of the high performance of the proposed method for aquifer parameters estimation. Moreover, investigation of the temporal behavior of the aquifer parameters enables us to predict the subsidence in near future which is as one of the innovative outcomes of the present study.

5. Conclusions

As an effective and novel method for inverse solution of groundwater flow equation, LBM combined with GA optimization was employed to determine the aquifer parameters including hydraulic conductivity (K), specific yield (S_y) and compressibility (α) in Darab plain. Using the compressibility relation in unconfined aquifer systems, the compressibility (α) at piezometric wells locations is estimated using the subsidence values measured by InSAR and hydraulic head measurements. A rough estimate of the specific yield (S_y) and sediment types are then approximated based on the compressibility values while the hydraulic conductivity (K) is obtained from the

existing reports. By considering the possible ranges of the aquifer parameters extracted from the previous step, the LBM combined with GA optimization is applied to precisely achieve the aquifer parameters. The optimization process tries to minimize the relative error between the calculated hydraulic head from LBM and the one computed using the subsidence value at every grid cell in the study area.

Thanks to annually estimation of the aquifer parameters, we are able to investigate their temporal behaviors. The decreasing trend of hydraulic conductivity and specific yield at most locations is an indication of the effect of land subsidence on the aquifer system properties. By fitting a function to time-dependent aquifer parameters at each grid cell, it is possible to predict the parameters in the near future which are further used to calculate the corresponding land subsidence. The small relative error between the predicted subsidence and the InSAR measurements demonstrates the significant performance of proposed method.

The temporal variation of the aquifer parameters suggests that the aquifer system is highly affected by the land subsidence. The compaction occurred in the fine-grained sediments results in the decreasing temporal trends observed in the specific yield and hydraulic conductivity values. This indicates an ongoing permanent reduction in the total storage capacity of the aquifer system which most probably leads to large surface runoff after a precipitation event. It means that the aquifer can no longer store water from the atmospheric predication. There is really a cause for severe concern specifically during drought events where people mostly rely on the groundwater resources. Precise information on the aquifer system properties and storability which is an outcome of this research, plays an important role for a successful groundwater management which is of important significance.

Acknowledgement

The authors wish to thank the Regional Water Company of Fars, Iran for their contribution in collecting the groundwater information.

References

Abdelaziz R, Merkel B (2015) Sensitivity analysis of transport modeling in a fractured gneiss aquifer. J Afr Earth Sci 103: 121–127. DOI:10.1016/j.jafrearsci.2014.12.003

Ansumali S, Karlin IV, Arcidiacono S, Abbas A, Prasianakis NI (2007) Hydrodynamics beyond Navier-Stokes: Exact Solution to the Lattice Boltzmann Hierarchy. Phys Rev Lett 98: 124502. https://doi.org/10.1103/PhysRevLett.98.124502

Anwar SH, Sukop MC (2008) Lattice Boltzmann Simulation of Solute Transport in Heterogeneous Porous Media with Conduits to Estimate Macroscopic Continuous Time Random Walk Model Parameters. Int J Comput Fluid Dyn 8 (8): 213-221.

Aral MM, Guan J, Maslia ML (2001) Identification of contaminant source location and release history in aquifers. J Hydrol Eng 6: 225–234. https://doi.org/10.1061/(ASCE)1084-0699(2001)6:3(225)

Arsyad MA, Ihsan N, Tiwow VA, Ahmar AS (2017) Model of groundwater flow using Boltzmann Lattice-Gas Automation method in Maros karst region, Indonesia, Drink. Water Eng Sci Discuss. 5(10): 65-72. DOI: https://doi.org/10.5194/dwes-2016-9

Ayaz MD (2017) Groundwater pollution source identification using genetic algorithm based optimization model. Int J Comput Sci 5: 65–72. DOI:10.26438/ijcse/v5i10.6572

Budinski L, Fabian J, Stipić M (2015) Lattice Boltzmann method for groundwater flow in non-orthogonal structured lattices. Comput Math With Appl 70: 2601–2615. https://doi.org/10.1016/j.camwa.2015.09.027

Fattahi E, Waluga C, Wohlmuth B, Rüde U, Manhart M, Helmig R (2016) Lattice boltzmann methods in porous media simulations: 339 From laminar to turbulent flow. Comput Fluids 140: 247 – 259. https://doi.org/10.1016/j.compfluid.2016.10.007

Gao Y, Yu Y, Yang L, Qin S, Hou G (2021) Development of a coupled simplified lattice Boltzmann method for thermal flows. Comput Fluids. 229: 105042. https://doi.org/10.1016/j.compfluid.2021.105042

Garcia L, Shigidi A (2007) Using neural networks for parameter estimation in ground water. J Hydrol 318: 215–231. https://doi.org/10.1016/j.jhydrol.2005.05.028

Gentry RW, Larsen D, Ivey S (2003) Efficacy of Genetic Algorithm to Investigate Small Scale Aquitard Leakage. J Hydraul Eng 129(7): 527-535. https://doi.org/10.1061/(ASCE)0733-9429(2003)129:7(527)

Geza M, Poeter E, McCray J (2009) Quantifying predictive uncertainty for a mountain-watershed model. J Hydrol (376): 170–181. DOI:10.1016/j.jhydrol.2009.07.025

Gharibi F, Ashrafizaadeh M (2020) Darcy and inertial fluid flow simulations in porous media using the non-orthogonal central moments lattice Boltzmann method. J Pet Sci Eng. https://doi.org/10.1016/j.petrol.2020.107572

Gladrow DW (1994) A lattice boltzmann equation for diffusion. J stat phys 79: 1023–1032. https://doi.org/10.1007/BF02181215

Hana K, Zuoa R, Nia P, Xuea Zh, Xua D, Wanga J, Zhang D (2020) Application of a genetic algorithm to groundwater pollution source identification. J Hydrol 589: 125343. DOI:10.1016/j.jhydrol.2020.125343

Hekmatzadeh AA, Adel A, Zarei F, Haghighi AT (2019) Probabilistic simulation of advection-reaction-dispersion equation using random lattice Boltzmann method. Int J Heat Mass Transf 144: 118647. https://doi.org/10.1016/j.ijheatmasstransfer.2019.118647

Hekmatzadeh AA, Keshavarzi H, Talebbeydokhti N, T.Haghighi A (2018) Lattice Boltzmann solution of advection-dominated mass transport problem: a comparison. Sci Iran 27(2): 625-638. 10.24200/sci.2018.5616.1376

Hoffmann J, Leake SA, Galloway DL, Wilson AM (2003) MODFLOW-2000, groundwater model- user guide to the subsidence and aquifer-system compaction (SUB) package. USGS, open-file report 03-233, Tucson, Arizona

Lei X, Qiao Y, Guo Z, Tian Y (2013) Stimulate the Pollutants Transport in Tai Lake with Lattice Boltzmann Method. Procedia Eng 61: 315-317

Lin Y, Yang C, Choi C, Zhang W, Machida H, Norinaga K (2021) Lattice Boltzmann simulation of multicomponent reaction-diffusion and coke formation in a catalyst with hierarchical pore structure for dry reforming of methane. Chem Eng Sci. 229: 116105. https://doi.org/10.1016/j.ces.2020.116105

Liu H, Zhou JG, Li M, Zhao Y (2013) Multi-block lattice Boltzmann simulations of solute transport in shallow water flows. Adv Water Resour. 58: 24-40. DOI:10.1016/j.advwatres.2013.04.008

Lu D, Ye M, Hill MC, Poeter EP, Curtis GP (2014) A computer program for uncertainty analysis integrating regression and Bayesian methods. Environ Model Softw (60): 45-56. https://doi.org/10.1016/j.envsoft.2014.06.002

Mahinthakumar GK, Sayeed M (2005) Hybrid genetic algorithm-local search methods for solving groundwater source identification inverse problems. J Water Res Plan 131: 45–57. https://doi.org/10.1061/(ASCE)0733-9496(2005)131:1(45)

Mohammad AA (2011) Lattice Boltzmann method: Fundamentals and engineering applications with computer codes. Springer Science & Business Media

Peng Y, Zhou JG, Burrows R (2011) Modelling solute transport in shallow water with the lattice Boltzmann method. Comput Fluids 50(1): 181-188. DOI:10.1016/j.compfluid.2011.07.008

Regional Water Company of Fars (2016) Prohibition of water extraction from Darab Plain. Report code 2722 (in Persian)

Ru Zh, Liu H, Xing L, Ding Y (2021) A well-balanced lattice Boltzmann model for the depth-averaged advection–diffusion equation with variable water depth. Comput Methods Appl Mech Eng 379: 113745. https://doi.org/10.1016/j.cma.2021.113745

Servan-Camas B, T-C.Tsai F (2009) Saltater intrusion modeling in heterogeneous confined aquifers using two-relaxation-time lattice Boltzmann method. Adv Water Resour 32(4): 620-631. DOI:10.1016/j.advwatres.2009.02.001

Sonnenborg T, Christensen B, Nyegaard P, Henriksen HJ, Refsgaard JC (2003) Transient modeling of regional groundwater flow using parameter estimates from steady-state automatic calibration. J Hydrol 273: 188–204. https://doi.org/10.1016/S0022-1694(02)00389-X

Sophia L, Bhattacharjya RK (2020) A GA based iterative model for identification of unknown groundwater pollution sources considering noisy data. Nature-Inspir. Methods Metaheuristics Optim https://doi.org/10.1007/978-3-030-26458-1_17

Yousefi R, Talebbeydokhti N, Afzali SH, Dehghani M (2019) Stress–strain analysis by genetic algorithm-based integration of longterm subsidence time series from different synthetic aperture radar platforms in Darab, Iran. J Appl Remote Sens 13(2): 024520. https://doi.org/10.1117/1.JRS.13.024520

Yousefi R, Talebbeydokhti N, Afzali SH, Hekmatzadeh AA (2021) A solution of unconfined groundwater flow with an innovative lattice Boltzmann method. Sci Iran 13 (2): 024520. 10.24200/sci.2021.55624.4321

Zhou JG (2004) Lattice Boltzmann Methods for Shallow Water Flows. Springer, United Kingdom. DOI:10.1002/fld.1489

Zhou JG (2007a) A lattice Boltzmann model for groundwater flows. Int J Mod Phys 18 (06): 973-991. https://doi.org/10.1142/S0129183107011078

Zhou JG (2007b) A rectangular lattice Boltzmann method for groundwater flows. Mod Phys Lett 21 (09): 531-542. https://doi.org/10.1142/S0217984907013080

Zhou JG (2011) Lattice Boltzmann method for advection and anisotropic dispersion equation. J Appl Mech78 (26): 1–5. https://doi.org/10.1115/1.4002572

Table.1 Information of Darab aquifer at piezometric wells (average value from 2010 to 2015)

well	*dh(m)*	*db(m)*	$\alpha(m^2/N)$	*S.T*	S_y
1	-4.83	-0.025	4.91E-09	gravel	0.23
2	-1.76	-0.121	4.51E-08	Medium sand	0.26
3	-0.26	-0.778	2.31E-06	Clay	0.07
4	-2.07	-0.046	2.25E-08	Dense sand	0.21
5	-1.41	-0.464	1.82E-07	Clay	0.07
6	-0.51	-0.012	3.14E-08	Medium sand	0.26
7	-5.87	-0.255	2.38E-08	Dense sand	0.21

8	-1.17	-0.017	9.15E-09	Sandy gravel	0.25
9	-0.68	-1.146	9.52E-07	Clay	0.07
10	-8.06	-0.054	6.07E-09	Sandy gravel	0.25
11	-0.86	-0.265	5.36E-07	Clay	0.07
12	-8.9	-0.053	3E-08	Medium sand	0.21

441

442

443

444 Table 2. Lower and upper bounds of the aquifer parameters used for GA optimization

Aquifer parameter	Lower bound	Upper bound
S_y	0.001	0.3
K (m/day)	0.08	20
α (m^2/N)	0.00	3E-7

445

446

447 Table 3. Model misfit as the relative error calculated at the locations of piezometric wells

Wells	Relative error (difference between observed and calculated hydraulic head)					
	2010 – 2011	2011 – 2012	2012 – 2013	2013 – 2014	2014 – 2015	2015 - 2016
W1	0.6E-3	0.6E-3	0.6E-3	0.6E-3	0.6E-3	0.6E-3
W2	0.8E-3	0.4E-3	0.5E-3	0.6E-3	0.6E-3	0.5E-3
W3	0.5E-3	0.4E-3	0.6E-3	0.5E-3	0.4E-3	0.4-3
W4	0.1E-3	0.4E-3	0.2E-3	0.2E-3	0.1E-3	0.6E-3
W5	0.6E-3	0.6E-3	0.7E-3	0.8E-3	0.7E-3	0.7E-3
W6	0.6E-3	0.4E-3	0.4E-3	0.4E-3	0.5E-3	0.5E-3
W7	0.4E-3	0.3E-3	0.2E-3	0.2E-3	0.2E-3	0.2E-3
W8	4E-05	0.1E-3	8E-05	5E-05	0.1E-3	9E-05
W9	0.5E-3	0.8E-3	0.8E-3	0.3E-3	0.4E-3	0.4E-3
W10	0.4E-3	0.1E-3	0.1E-3	0.1E-3	0.1E-3	5E-05
W11	0.2E-3	0.1E-3	0.1E-3	2E-05	1E-05	0.1E-3
W12	0.7E-3	0.7E-3	0.7E-3	0.7E-3	0.7E-3	0.7E-3

448

449

450

451

452

453

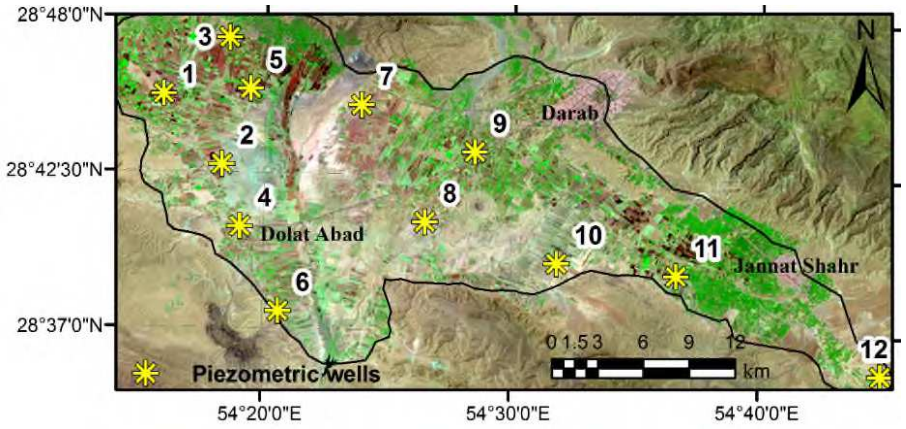

Fig.1. Location of the aquifer system in the Darab plain superimposed on the LANDSAT 8 OLI color composite image (R:7, G:4, B:2). The yellow stars represent the piezometric wells while the green areas in the black polygon indicate the agricultural lands

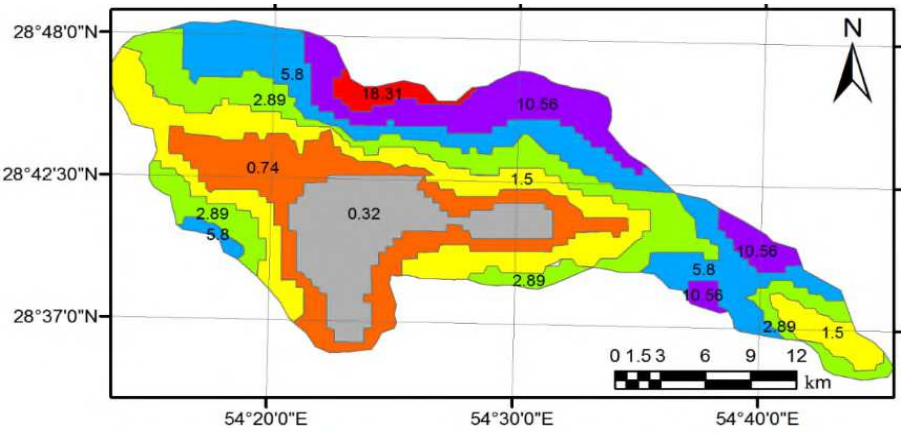

Fig.2. Initial hydraulic conductivity (m/day) of Darab aquifer system

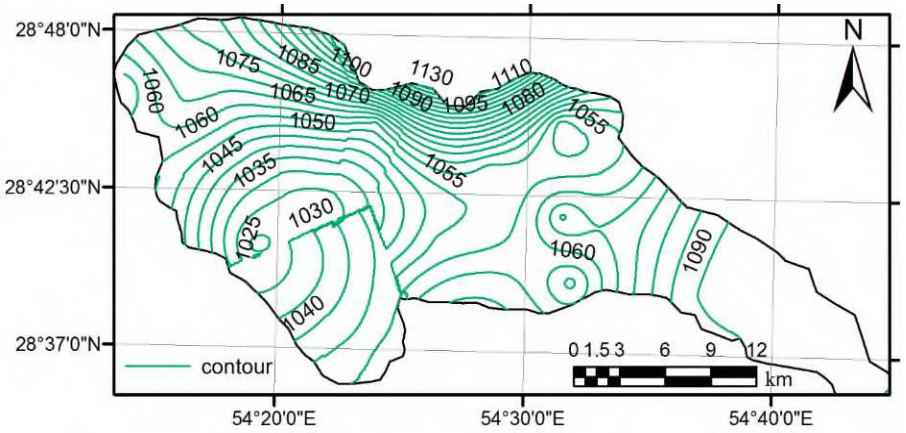

Fig.3. Hydraulic head in Darab aquifer system

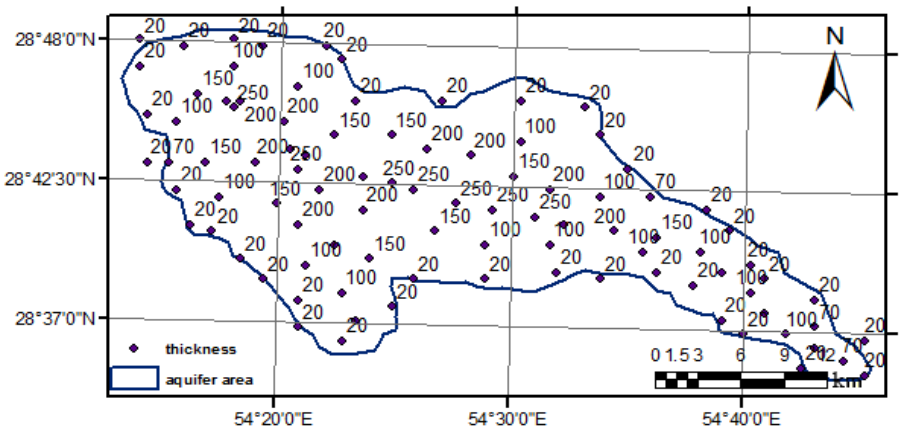

Fig.4. Thickness (m) of Darab aquifer system

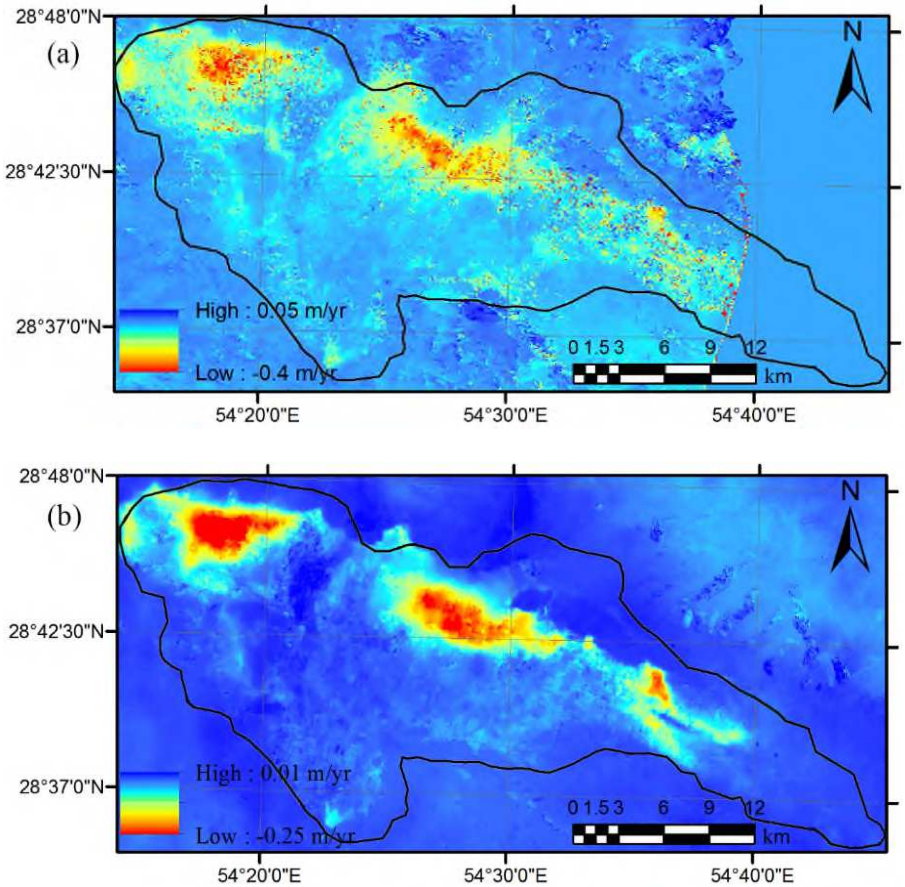

Fig.5. Subsidence velocity maps obtained from: (a) ENVISAT ASAR and (b) Sentinel-1A (Yousefi et al. 2019)

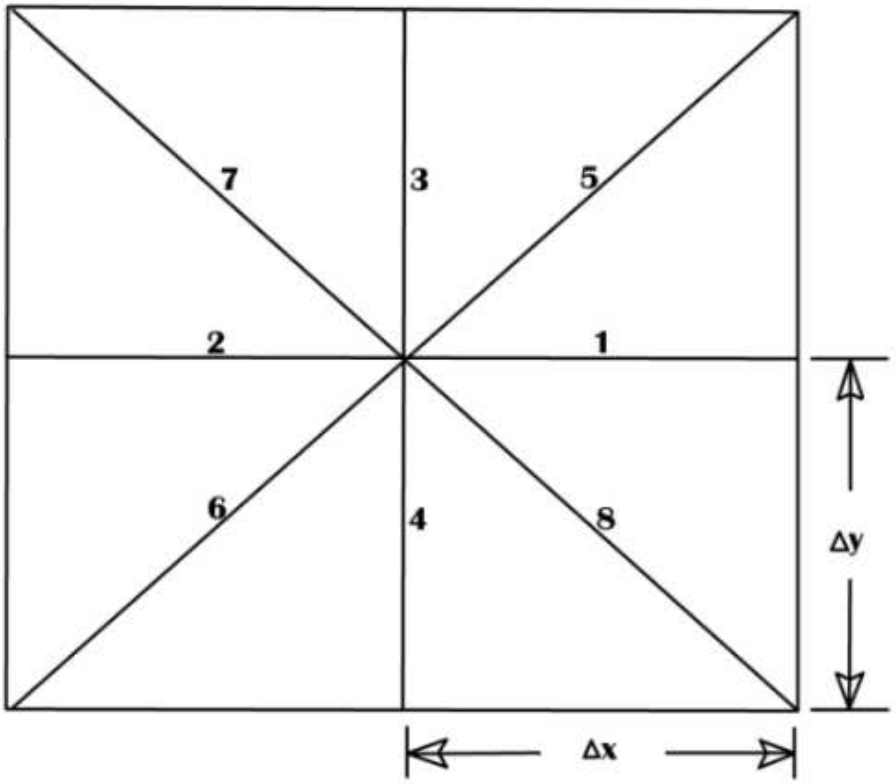

Fig.6. Nine-velocity rectangular lattice (D2Q9) (Mohammad 2011)

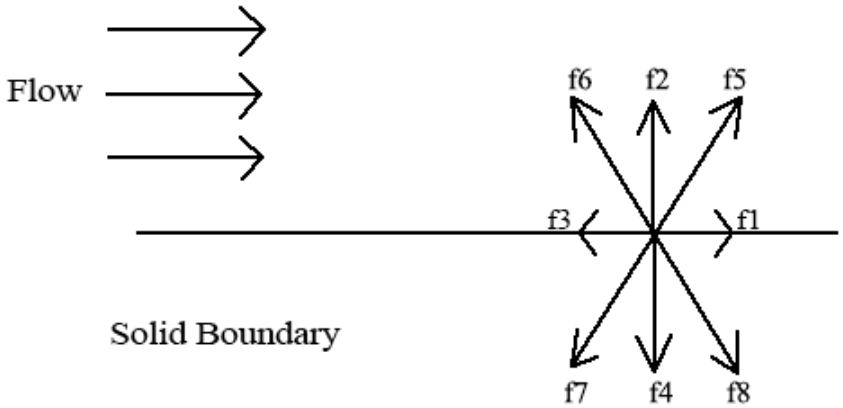

Fig.7. Solid boundary condition (Mohammad 2011)

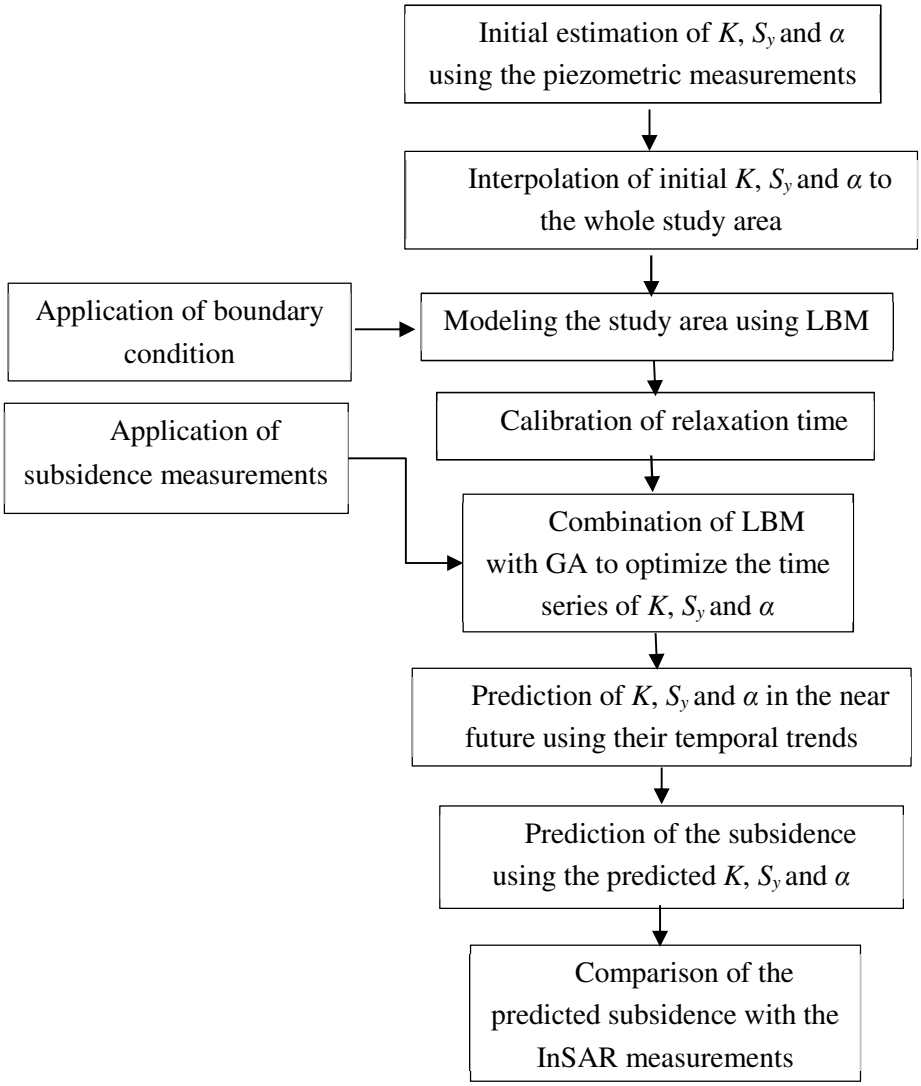

Fig.8. Block diagram of the proposed methodology for aquifer parameters estimation

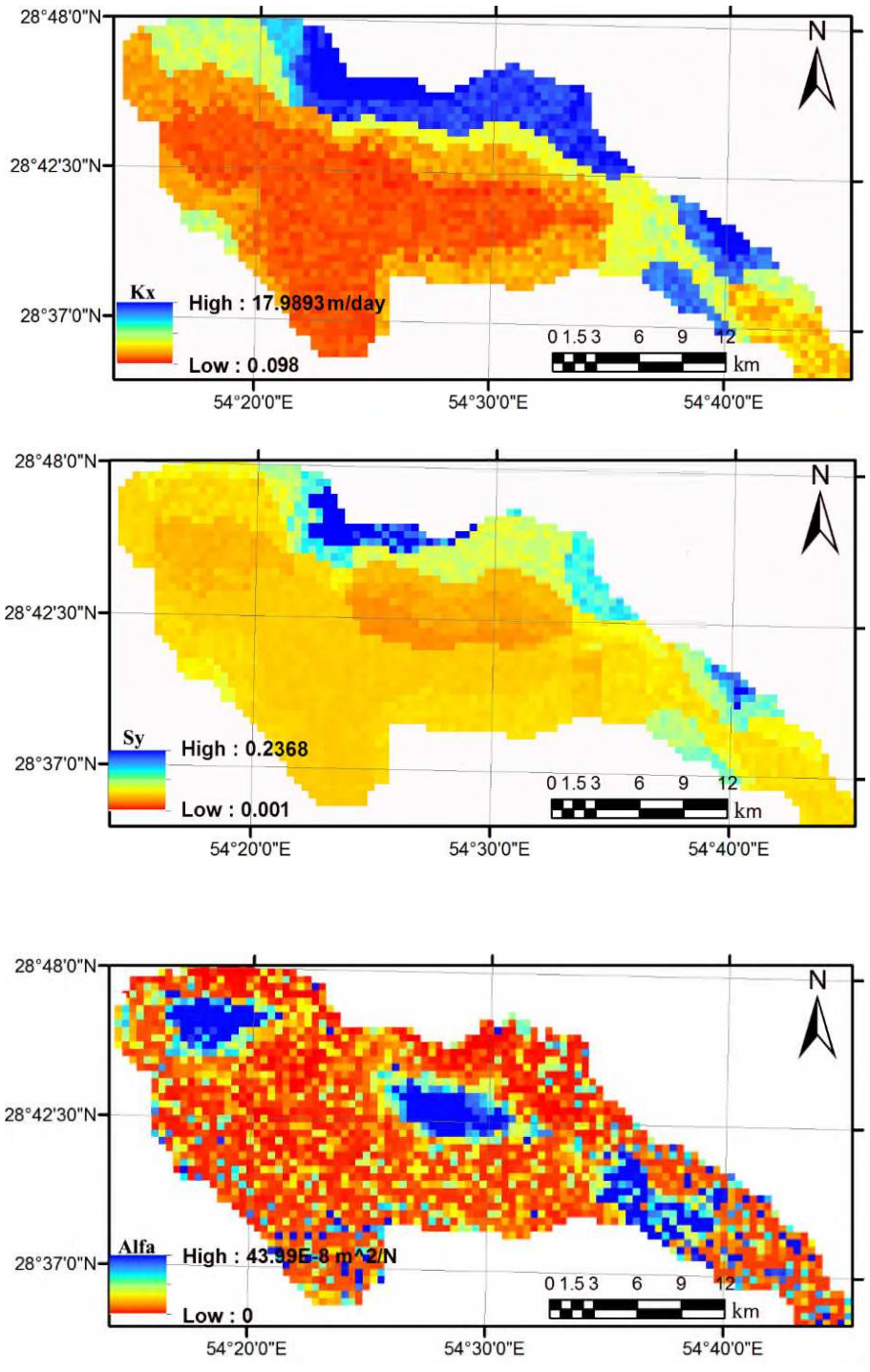

522

523

524

525

526 Fig.9. Optimized K, S_y and α in 2010-2011

527

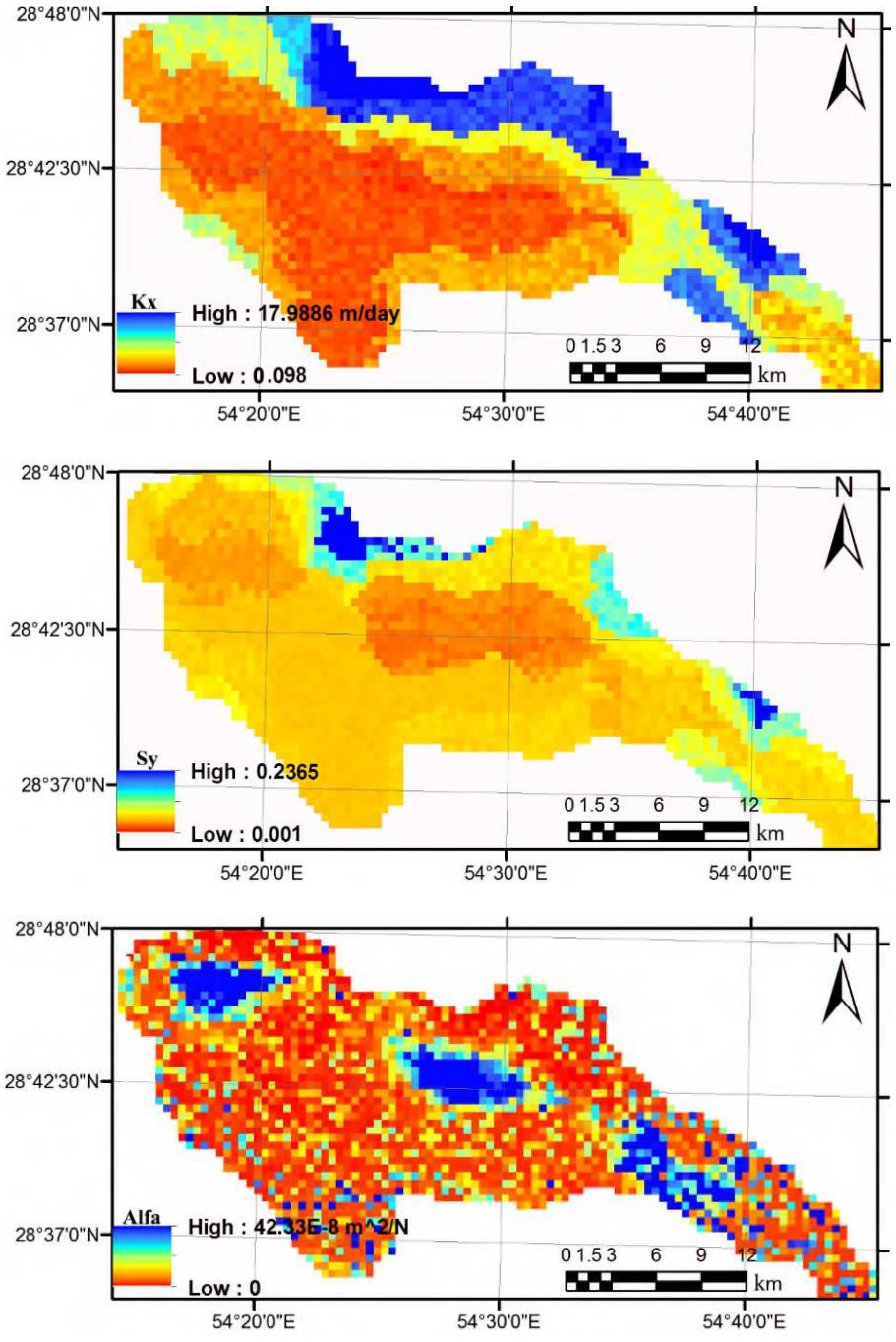

Fig.10. Optimized K, S_y and α in 2011-2012

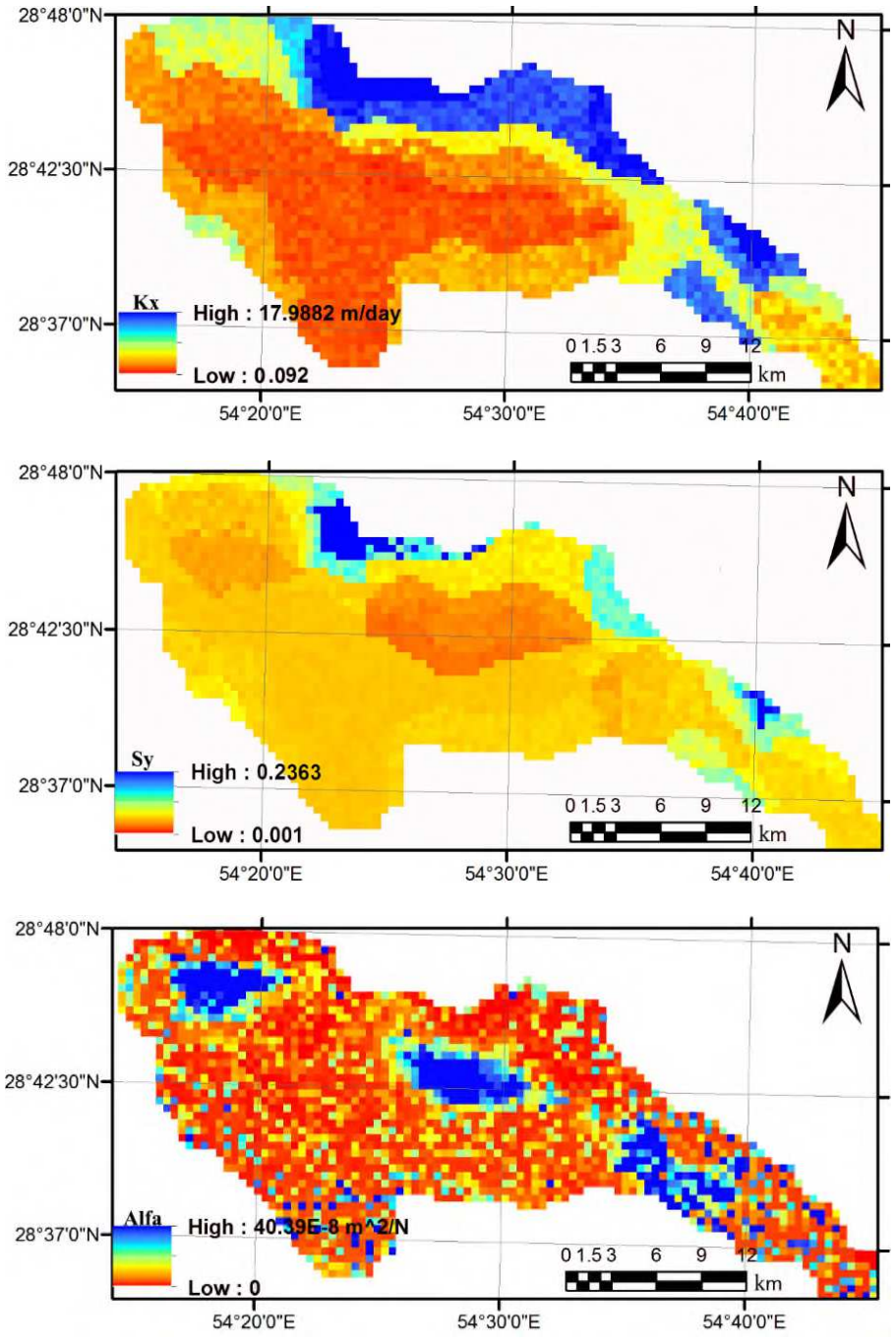

533

534

535

536 Fig.11. Optimized K, S_y and α in 2012-2013

537

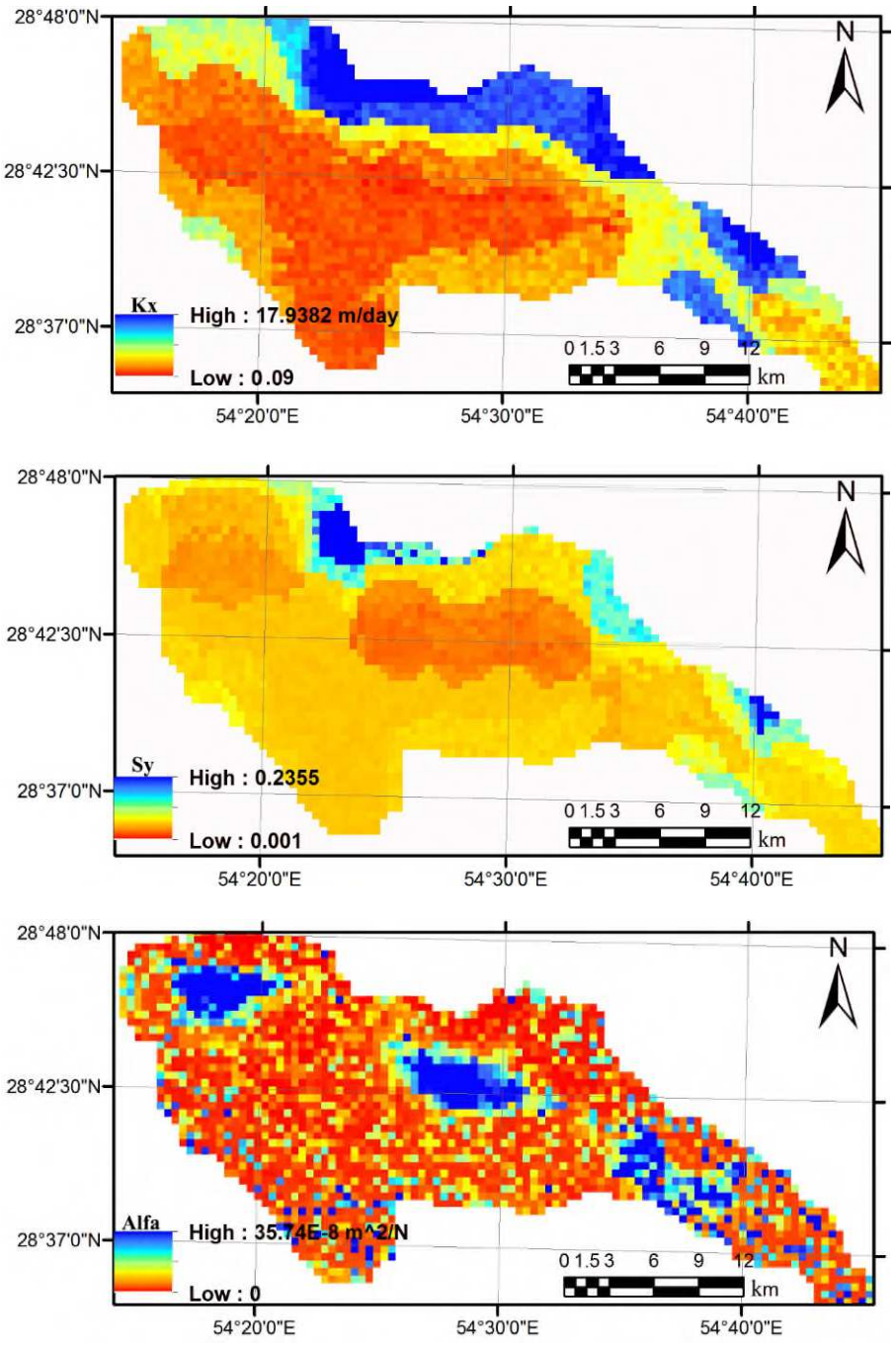

Fig.12. Optimized K, S_y and α in 2013-2014

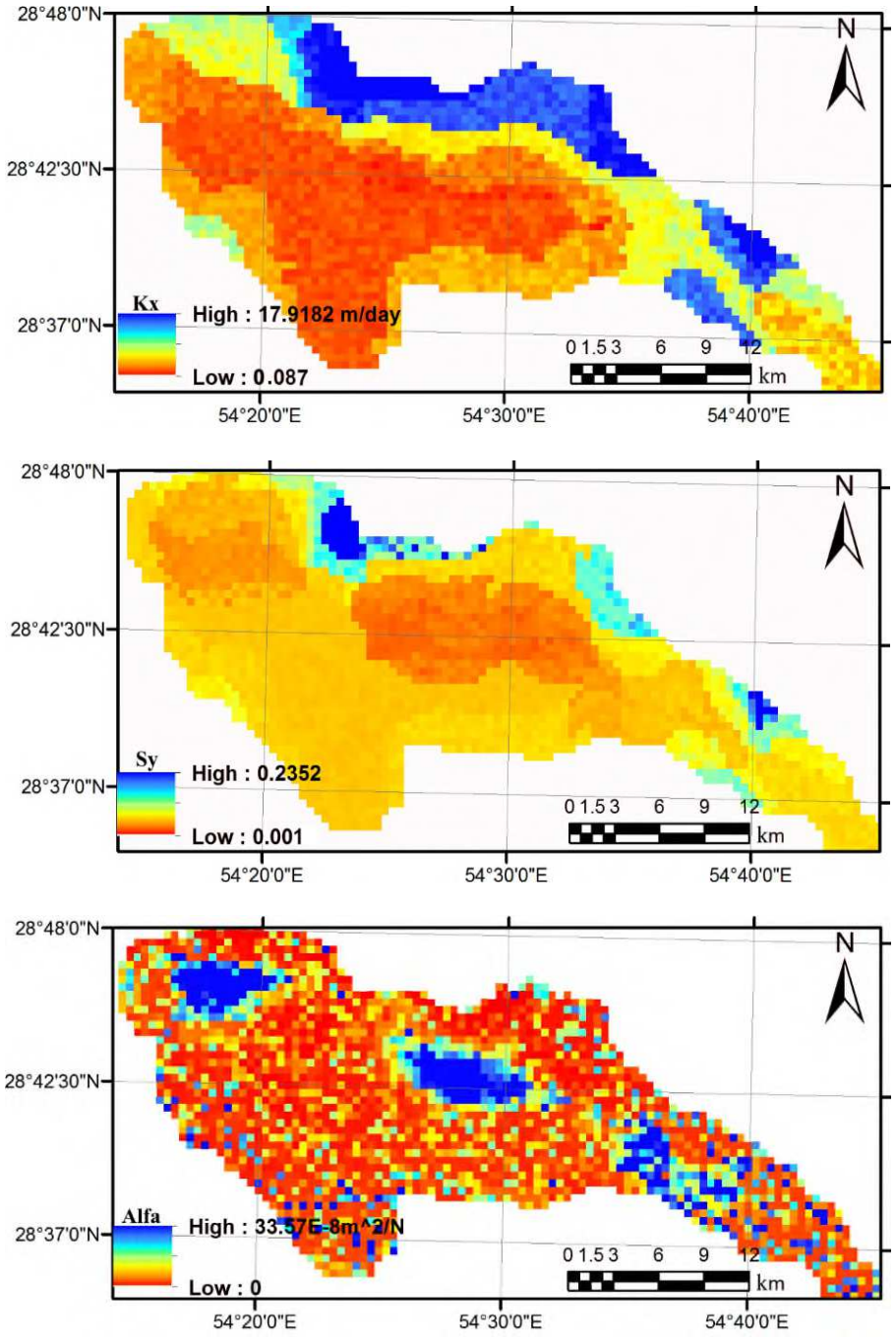

Fig.13. Optimized K, S_y and α in 2014-2015

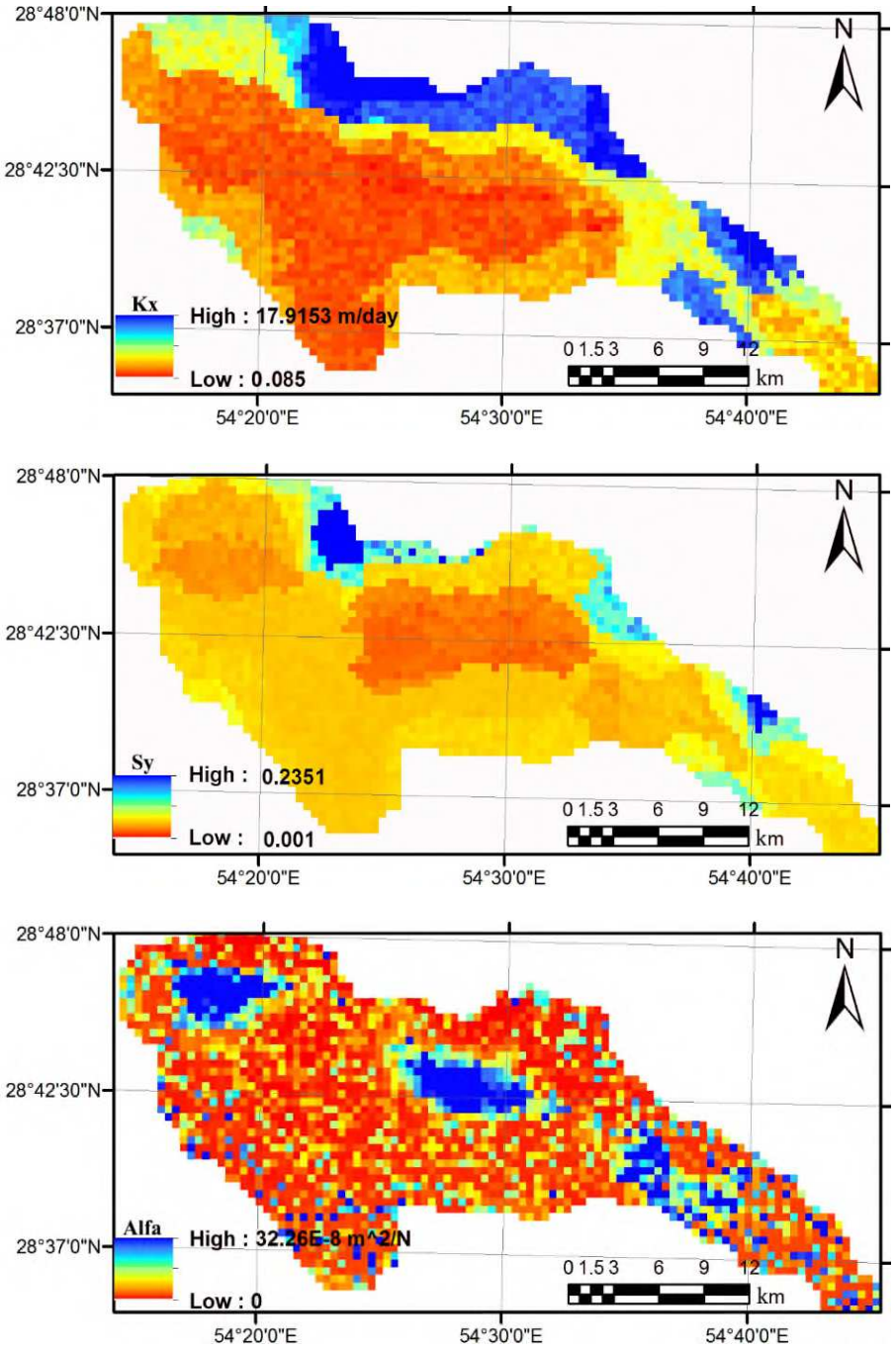

Fig.14. Optimized K, S_y and α in 2015-2016

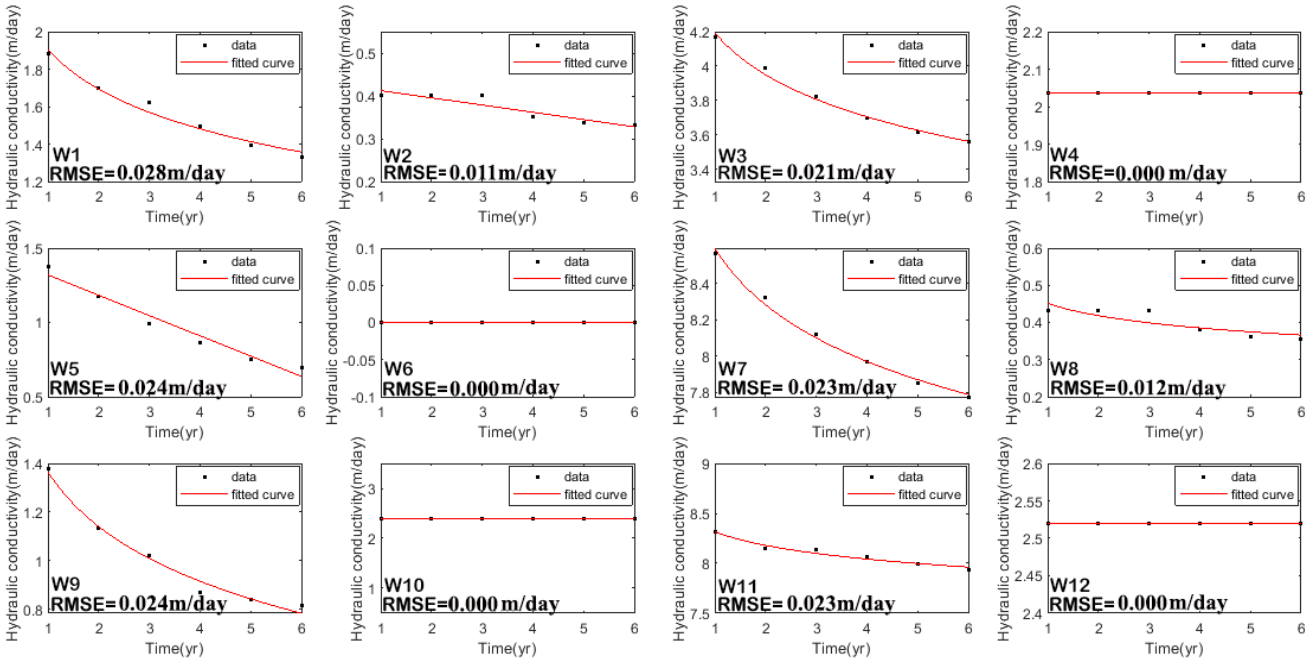

Fig.15. Model fitted to the values of hydraulic conductivity (k_x) at the locations of piezometric wells in 2010-2016. Solid line illustrates the temporal model.

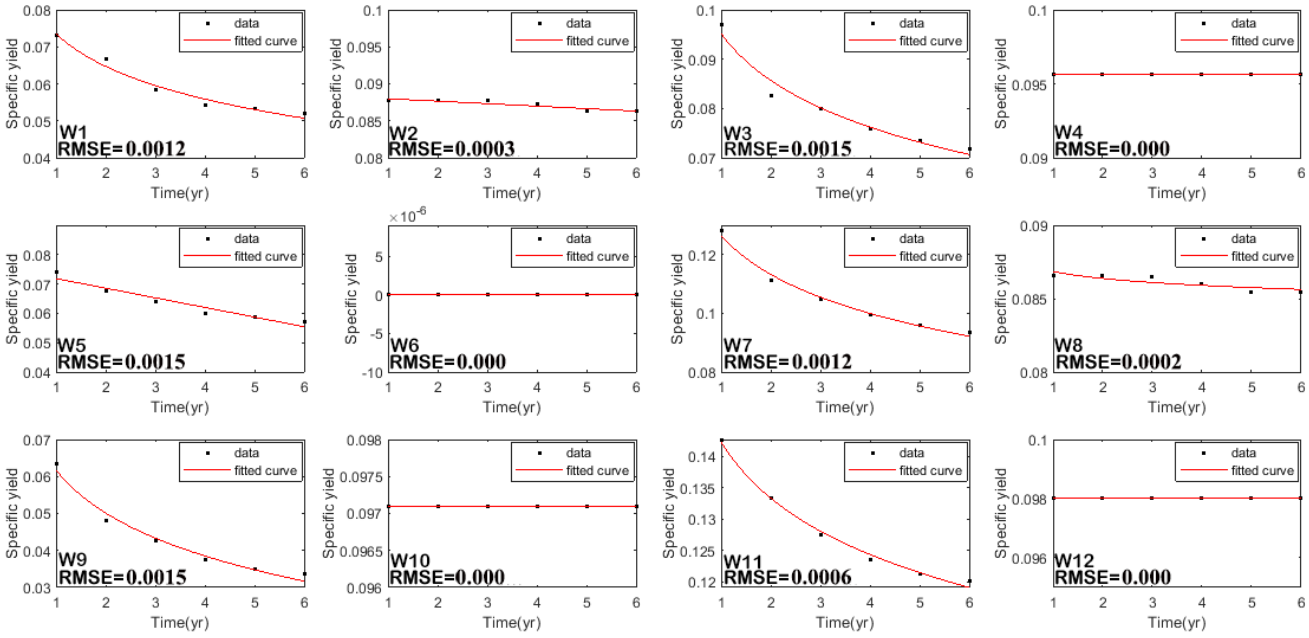

Fig.16. Model fitted to the values of specific yield (S_y) at the locations of piezometric wells in 2010-2016. Solid line illustrates the temporal model.

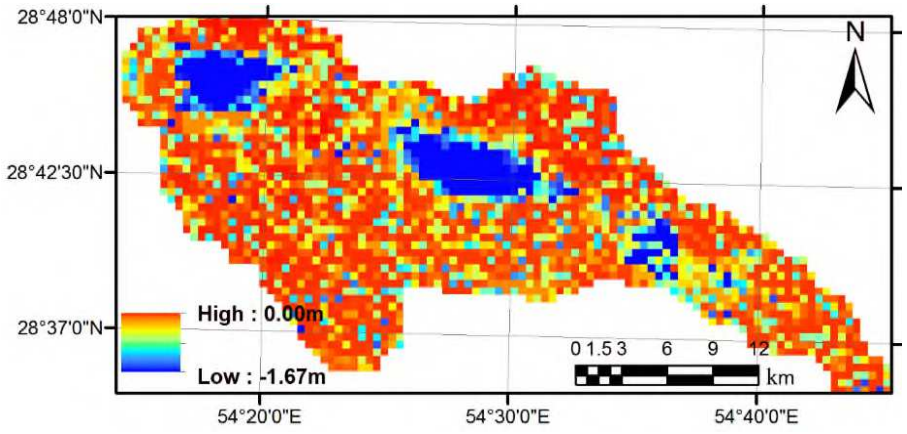

Fig.18. Predicted subsidence using the anticipated values of the aquifer parameters in 2017

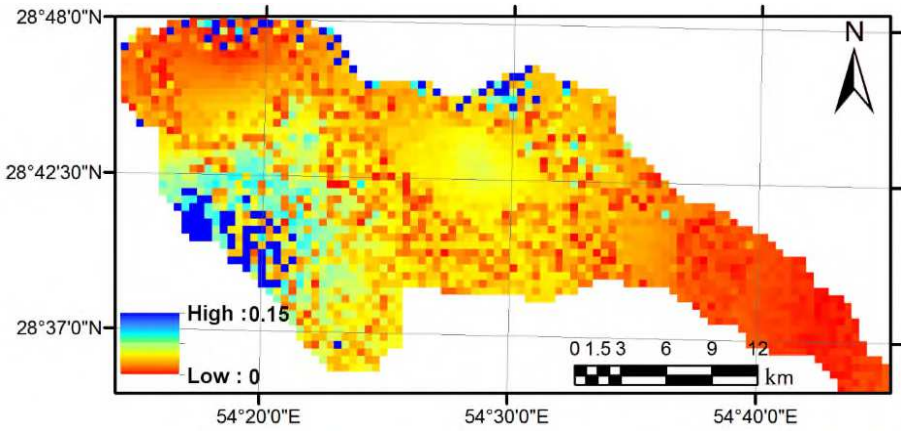

Fig. 19. Relative error between the predicted subsidence and InSAR measurements

Supplementary Files

This is a list of supplementary files associated with this preprint. Click to download.

- MyGraphicalAbstract2.tif